

## Chapter 5

# Volume Scattering Function and Backscattering Coefficients: Instruments, Characterization, Field Measurements and Data Analysis Protocols

J. Ronald V. Zaneveld<sup>1</sup>, Scott Pegau<sup>1</sup> and James L. Mueller<sup>2</sup>

<sup>1</sup>*College of Oceanographic and Atmospheric Sciences, Oregon State University, Corvallis*

<sup>2</sup>*Center for Hydro-Optics and Remote Sensing, San Diego State University, California*

### 5.1 INTRODUCTION

The volume scattering function (VSF)  $\beta(\lambda, \psi)$  [ $\text{sr}^{-1}\text{m}^{-1}$ ] and the volume absorption coefficient  $a(\lambda)$  [ $\text{m}^{-1}$ ] provide the most fundamental description of a medium's inherent optical properties (IOP), as all other IOP can be derived from them. In particular, the volume scattering coefficient  $b(\lambda)$  and volume backscattering coefficient  $b_b(\lambda)$  may be derived by integrating  $\beta(\lambda, \psi)$  over the unit sphere and backward hemisphere, respectively. In terms of determining the "complete" IOP from *in situ* measurements, a useful combination is  $a(\lambda)$ , the beam attenuation coefficient  $c(\lambda)$ , and the volume scattering phase function  $\beta(\lambda, \psi) = \frac{\beta(\lambda, \psi)}{c(\lambda) - a(\lambda)}$ . The reader is referred to Vol. I, Chapter 2 (Sect. 2.4) and to Chapter 1 of the present volume for further details regarding these definitions and relationships.

Knowledge of the VSF is a critical prerequisite to accurate radiative transfer modeling of remote sensing reflectance and water-leaving radiance. In Vol. III, Chapter 4 (and references cited there), it is shown that irradiance reflectance  $R(\lambda)$  is approximately proportional to the ratio of the backscattering to absorption coefficients, and that upwelled radiance just beneath the sea surface is proportional to  $R(\lambda)$ , so that

$$L_u(0^-, \lambda, \theta, \phi) = E_d(0^-, \lambda) \frac{f b_b(\lambda)}{Q a(\lambda)}.$$

This relationship is completely general and exact, but it does not express a linear proportionality to the IOP ratio, because the factors  $f$  and  $Q$  are not simply coefficients. They are functions,  $f[\lambda, (\theta_o, \tau_a, W), a(\lambda), \beta(\lambda, \Psi)]$  and  $Q[(\lambda, \theta', \phi), (\theta_o, \tau_a, W), a(\lambda), \beta(\lambda, \Psi)]$ , that account for the bidirectional nature of the ocean's reflectance; this bidirectionality may be traced directly to the shape of the VSF. Bidirectionality of remote sensing reflectance, as it arises from the VSF, is shown more explicitly in the formulation by Zaneveld (1982).

Equation (1.18) could be used directly as a basis for measuring the VSF if an instrument's source and detector were well collimated, and there were no flux losses, or FOV distortions, associated with an its optical elements. Some general angle scattering meters (Petzold 1972; Lee *et al.* 2003) are designed with a well-enough collimated beam and very small detector acceptance angle, so that equation (1.18) may be applied directly. In terms of equation (1.19), this is equivalent to assuming that the scattering response weighting function  $W(\lambda, \psi, \phi; c)$  is narrow enough to set it to unity. The General Angle Scattering Meter (GASM), built at the Scripps Institution of Oceanography's Visibility Laboratory (Petzold 1972), consists

of a lamp focused into a cylindrical beam, and a narrow field of view detector mounted to swing in an arc to view the beam at many off-axis scattering angles between approximately  $10^\circ$  and  $170^\circ$ . Petzold (1972) reported VSF's measured for selected natural waters using the (GASM). This reference has been widely used to describe shapes of  $\beta(\lambda, \psi)$  in natural waters. Mobley *et al.* (2001) compared measured and modeled nadir-viewing remote sensing reflectances, using measured  $c(\lambda)$  and  $a(\lambda)$  with  $\beta(\lambda, \psi)$  of different assumed shapes, including that of Petzold (1972), and the VSF measured using a general angle scattering meter of a new design (Lee *et al.*, 2003); best agreement was achieved using the measured VSF. Their results showed that large systematic offsets can result if one arbitrarily assumes a scattering phase function having an incorrect backward scattering fraction. The results of Mobley *et al.* (2001) also indicated that nadir-viewing radiance reflectance is less sensitive to the detailed shape of the forward scattering lobe of  $\beta(\lambda, \psi)$ . Details of scattering at intermediate forward angles might, however, be more important for off-nadir viewing geometry (Vol. III, Ch. 4).

At present, commercially available VSF sensors<sup>1</sup> are designed with detector beam-spread and detector acceptance angles ranging from  $10^\circ$  to  $20^\circ$  Full-Width Half-Maximum (FWHM). These instruments measure the VSF, weighted as in (1.19), at one (or a few) scattering angle(s) and are typically used to determine the backscattering coefficient using the methods described below in Sect. 5.4. Although these methods depend on assumptions concerning  $\beta(\lambda, \psi)$ , determinations of  $b_b(\lambda)$  from VSF profile measurements with these instruments, when combined with absorption and beam attenuation coefficients, radiometric profiles and pigment concentration measurements, have provide useful information about relationships between IOP, AOP and optically important material constituents of the water column (*e.g.* Stramska *et al.* 2000).

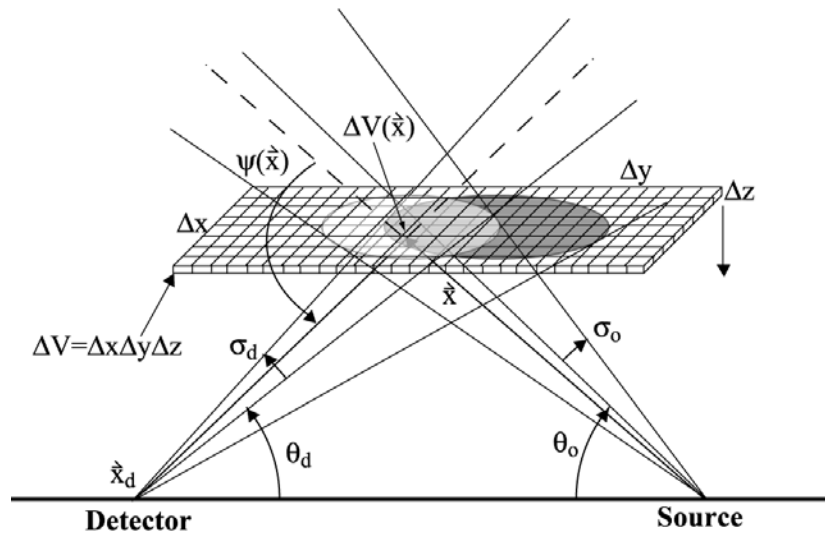


Fig. 5.1: Schematic illustration of a VSF sensor geometry used for numerical integration over the volume intersected by a source beam and detector FOV of incremental elements of the

<sup>1</sup> Certain commercial equipment, instruments, or materials are identified in this chapter to foster understanding. Such identification does not imply recommendation, or endorsement, by the National Aeronautics and Space Administration, nor does it imply that the materials or equipment identified are necessarily the best available for the purpose.

scattered radiant flux received by the detector.

An example of a generalized source and detector arrangement to measure the VSF  $\beta(\lambda, \psi)$  at a scattering angle  $\psi > \frac{\pi}{2}$  is illustrated schematically in Fig. 5.1. To determine a calibration factor relating the detector response to flux scattered from the source beam into the field of view (FOV) of the detector, we must determine the sensor's response weighting function  $W(\lambda, \psi, \varphi; c)$  [equation (1.19)], either explicitly, or implicitly. The explicit approach to this problem is to determine  $W(\lambda, \psi, \varphi; c)$  from geometry and first principles, and then calibrate the instrument's response signals in a medium having a known VSF  $\beta(\lambda, \psi)$ ; the detailed steps in this approach are described below in Sect. 5.2. The implicit approach (Maffione and Dana 1997) is to insert a plaque of known near-Lambertian reflectance in the position of the horizontal  $xy$ -plane, at distance  $z$  from the source-detector axis, illustrated Fig. 5.1, and record the instrument's responses as the plaque is moved vertically in small increments through the volume defined by the intersection of the source beam and detector FOV; this approach is briefly outlined in Sect. 5.3 below, but the reader is referred to Maffione and Dana (1997) for the detailed derivation and method of implementation.

For brevity, we will henceforth omit the explicit wavelength dependence of variables.

## 5.2 CHARACTERIZATION AND CALIBRATION OF A VSF SENSOR FROM ITS GEOMETRY AND RESPONSE TO SCATTERING BY POLYSTYRENE BEADS

### *Geometric Determination of $W(\psi)$*

Figure 5.1 illustrates a source located at the origin  $\mathbf{x}_o = (0, 0, 0)$  and a detector located on the  $y$ -axis at position  $\mathbf{x}_d = (0, y_d, 0)$ . As illustrated, the source beam and detector FOV are assumed to be cones with divergence angles  $\sigma_o$  and  $\sigma_d$ , respectively. At a distance  $z$  above the  $xy$  plane, a horizontal plane is shown passing through the source beam (a nearly transparent, light-shaded ellipse) and detector FOV (a dark shaded ellipse); the intersection of the source beam and detector FOV is the intermediate gray-shaded area. The plane is divided into elemental volume elements  $\Delta V = \Delta x \Delta y \Delta z$ , and a particular volume element is denoted  $\Delta V(\mathbf{x})$ .

The radiant flux  $\Phi_o$  emitted by the source is assumed to be evenly distributed over the solid angle  $\Omega_o$ , so by definition, the source radiant intensity is, by definition  $I_o = \left( \frac{\Phi_o}{\Omega_o} \right)$ . The flux transmitted in direction  $\hat{\mathbf{e}}(\mathbf{x}) = \frac{1}{|\mathbf{x}|} \mathbf{x}$ , where the vector length  $|\mathbf{x}| = \sqrt{\mathbf{x} \mathbf{g} \mathbf{x}}$ , from the source to the elemental volume  $\Delta V(\mathbf{x})$  is

$$\Delta \Phi_o [\Delta V(\mathbf{x}); c] = I_o \Delta \Omega_o [\Delta V(\mathbf{x})] \exp(-c|\mathbf{x}|) = \Phi_o \frac{\Delta \Omega_o [\Delta V(\mathbf{x})]}{\Omega_o} \exp(-c|\mathbf{x}|), \quad (5.1)$$

where  $\Delta \Omega_o [\Delta V(\mathbf{x})] = \frac{\Delta x \Delta y |\hat{\mathbf{e}}(\mathbf{x}) \mathbf{g} \hat{\mathbf{n}}|}{|\mathbf{x}|^2}$  is the solid angle subtended at the source by the horizontal elemental area  $\Delta x \Delta y$  at position  $\mathbf{x}$ , and  $\hat{\mathbf{n}}$  is the unit normal to the  $xy$ -plane (Fig. 5.1). Thus, the irradiance incident on  $\Delta V(\mathbf{x})$  is

$$E_o(\mathbf{x};c) = \frac{\Phi_o}{\Delta x \Delta y} |\hat{\mathbf{e}}(\mathbf{x}) \mathbf{g}\hat{\mathbf{n}}| \frac{\Delta \Omega_o [\Delta V(\mathbf{x})]}{\Omega_o} \exp(-c|\mathbf{x}|). \quad (5.2)$$

The radiant flux intensity scattered from  $\Delta V(\mathbf{x})$  in direction  $\hat{\mathbf{e}}(\mathbf{x}_d - \mathbf{x})$  toward the detector at  $\mathbf{x}_d$  is

$$I_s[\psi(\mathbf{x})] = \beta[\psi(\mathbf{x})] E_o(\mathbf{x}) \Delta V, \quad (5.3)$$

where the scattering angle  $\psi(\mathbf{x})$  for the incremental volume element is

$$\cos[\psi(\mathbf{x})] = \hat{\mathbf{e}}(\mathbf{x}) \mathbf{g}\hat{\mathbf{e}}(\mathbf{x}_d - \mathbf{x}). \quad (5.4)$$

Combining (5.2) and (5.3), and multiplying by the flux transmittance over the pathlength  $|\mathbf{x}_d - \mathbf{x}|$  leads to

$$\frac{\Delta \Phi_d [\Delta V(\mathbf{x});c]}{\Phi_o} = \beta[\psi(\mathbf{x})] \frac{\Delta V}{\Delta x \Delta y} |\hat{\mathbf{e}}(\mathbf{x}) \mathbf{g}\hat{\mathbf{n}}| \frac{\Delta \Omega_o [\Delta V(\mathbf{x})] \Delta \Omega_d [\Delta V(\mathbf{x})]}{\Omega_o} \exp[-c(|\mathbf{x}| + |\mathbf{x}_d - \mathbf{x}|)], \quad (5.5)$$

where the solid angle subtended by the area  $\Delta x \Delta y$  at the detector is  $\Delta \Omega_d [\Delta V(\mathbf{x})] = \frac{\Delta x \Delta y |\hat{\mathbf{e}}(\mathbf{x}_d - \mathbf{x}) \mathbf{g}\hat{\mathbf{n}}|}{(\mathbf{x}_d - \mathbf{x}) \mathbf{g}(\mathbf{x}_d - \mathbf{x})}$ .

With reference to (1.18) through (1.20), we may now write

$$\frac{\Delta \Phi_d [\Delta V(\mathbf{x});c]}{\Phi_o} = \beta[\psi(\mathbf{x})] W(\mathbf{x};c), \quad (5.6)$$

and by substitution we obtain the incremental weighting function for each volume element  $\Delta V(\mathbf{x})$  as

$$W(\mathbf{x};c) = \frac{\Delta V}{\Delta x \Delta y} |\hat{\mathbf{e}}(\mathbf{x}) \mathbf{g}\hat{\mathbf{n}}| \frac{\Delta \Omega_o [\Delta V(\mathbf{x})] \Delta \Omega_d [\Delta V(\mathbf{x})]}{\Omega_o} \exp[-c(|\mathbf{x}| + |\mathbf{x}_d - \mathbf{x}|)]. \quad (5.7)$$

To obtain the desired weighting function  $W(\psi;c)$  for each scattering angle  $\psi$  it is necessary to sum the weights for all volume elements at which the scattering angle falls within a discrete angular interval of  $\psi$ , *i.e.*

$$W(\psi;c) = \sum_x \sum_y \sum_z W(\mathbf{x};c) \delta[\psi, \psi(\mathbf{x}), \Delta \psi] \quad (5.8)$$

where

$$\delta[\psi, \psi(\mathbf{x}), \Delta \psi] = \begin{cases} 1; & \psi - \frac{\Delta \psi}{2} < \psi(\mathbf{x}) \leq \psi + \frac{\Delta \psi}{2} \\ 0; & \text{Otherwise} \end{cases}. \quad (5.9)$$

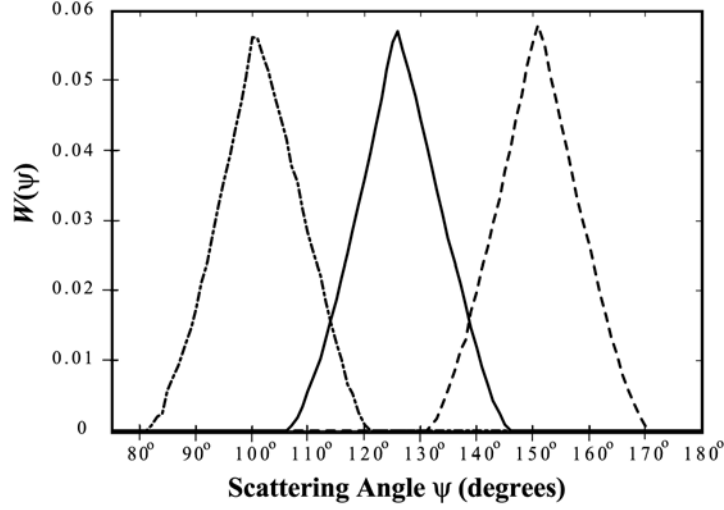


Figure 5.2: Examples of weighting functions  $W(\psi)$  calculated for VSF measurements by source-detector pairs aligned at nominal scattering angles  $(\bar{\psi}_1, \bar{\psi}_2, \bar{\psi}_3) = (100^\circ, 125^\circ, 150^\circ)$  (Figs. 5.1 and 1.4).

Once the weighting functions are computed for all scattering angles  $\psi$  falling within the beam and detector FOV intersection volume, they are normalized such that

$$\sum_{\psi} W(\psi; c) = 1. \quad (5.10)$$

As an example, the weighting functions calculated for the WET Labs VSF-3 are illustrated in Fig. 5.2 for nominal scattering angles  $(\bar{\psi}_1, \bar{\psi}_2, \bar{\psi}_3) = (100^\circ, 125^\circ, 150^\circ)$ . These particular, triangular source functions were derived assuming that both the source beam and detector FOV are conical about the respective centerlines illustrated in Fig. 5.1.

#### *Generalized Weighting Functions for Arbitrary Source Beam and Detector FOV Geometries*

In the above development of equations (5.1) through (5.7), it was assumed that the flux emitted by the source was uniformly distributed over a conical beam with its axis directed in direction

$$\hat{\mathbf{e}}_o = \begin{bmatrix} \sin\left(\frac{\pi}{2} + \theta_o\right) \\ 0 \\ \cos\left(\frac{\pi}{2} + \theta_o\right) \end{bmatrix},$$

and that the detector flux responsivity was also uniformly distributed over a conical FOV having its axis aligned in direction

$$\hat{\mathbf{e}}_d = \begin{bmatrix} -\sin\left(\frac{\pi}{2} + \theta_d\right) \\ 0 \\ \cos\left(\frac{\pi}{2} + \theta_d\right) \end{bmatrix}.$$

We may generalize the vector solid angle associated with the source beam as  $\hat{\Omega}_o^V$ , which represents the angular solid angle domain, measured relative to  $\hat{\epsilon}_o$ , over which flux emitted by the source is non-zero. Similarly,  $\hat{\Omega}_d^V$  is the solid angle domain relative to  $\hat{\epsilon}_d$  over which the detector's responsivity is non-zero. There are no restrictions on either the patterns of angular limits associated with  $\hat{\Omega}_o^V$  and  $\hat{\Omega}_d^V$ , or on the relative distributions of flux within  $\hat{\Omega}_o^V$ , or of flux responsivity within  $\hat{\Omega}_d^V$ .

Real sources generally emit flux in a somewhat irregular beam pattern that typically peaks in the vicinity of  $\hat{\epsilon}_o$ , may be relatively flat for much of its FWHM beam width, and then tends to fall sharply near the edges of the beam and gradually decay beyond the nominal FWHM limits. Detector angular responsivity FOV patterns generally exhibit similar geometric characteristics relative to  $\hat{\epsilon}_d$ .

The flux variations within the source beam may be expressed as a normalized relative flux distribution function  $h_o[\hat{\epsilon} \in \hat{\Omega}_o^V]$  that takes non-zero values only in directions included in the solid angle beam pattern. Similarly, the angular response function of the the detector may be written  $h_d[\hat{\epsilon} \in \hat{\Omega}_d^V]$ . To generalize the weighting functions to account for arbitrary source beam and detector FOV geometries, and relate the phase function to incremental detector responses  $\Delta D_d[\Delta V(\hat{\mathbf{x}}); c]$ :

1. Multiply the right-hand-sides of equations (5.1) and (5.2) by  $h_o[\hat{\epsilon}(\hat{\mathbf{x}}) \in \hat{\Omega}_o^V]$ , and carry this factor through subsequent substitutions.
2. Substitute using the relationship  $\Delta D_d[\Delta V(\hat{\mathbf{x}}); c] = h_d[-\hat{\epsilon}(\hat{\mathbf{x}}_d - \hat{\mathbf{x}}) \in \hat{\Omega}_d^V] \Delta \Phi_d[\Delta V(\hat{\mathbf{x}}); c]$  on the left-hand-side of (5.7) to relate  $\beta[\psi(\hat{\mathbf{x}})]$  to the incremental detector response.
3. Absorb the source flux and detector responsivity distributions into the weighting function  $W(\hat{\mathbf{x}}; c)$  by multiplying the right-hand-side of (5.7) by the product  $h_o[\hat{\epsilon}(\hat{\mathbf{x}}) \in \hat{\Omega}_o^V] h_d[-\hat{\epsilon}(\hat{\mathbf{x}}_d - \hat{\mathbf{x}}) \in \hat{\Omega}_d^V]$ .

The numerical implementation of the general form of (5.7) is straightforward. The more difficult aspect of obtaining generalized weighting functions is the experimental determination of the functions  $h_o[\hat{\epsilon} \in \hat{\Omega}_o^V]$  and  $h_d[\hat{\epsilon} \in \hat{\Omega}_d^V]$ .

The detector FOV responsivity distribution function may be measured by mounting the detector in a rotating stage, with its entrance aperture centered on the intersection of the axis of rotation and the optical axis of a stable collimated source. The stage is rotated in small angular increments, and the detector response is recorded at each angle to measure the relative variations in response in one plane containing  $\hat{\epsilon}_d$ . The instrument is then rotated in increments about  $\hat{\epsilon}_d$  and the process is repeated to map the distribution of responses in a sequence of planes adequate to resolve the full function  $h_d[\hat{\epsilon} \in \hat{\Omega}_d^V]$ . This is essentially the same procedure used to characterize the angular FOV of field radiometers (Vol. II, Ch. 3).

The inverse of the above setup may be used to map the flux distribution of the source beam. The instrument is mounted with the source aligned with the optical and rotation axes, and a narrow FOV detector is substituted for the collimated source. The stage is rotated through a suitable angular range to map out flux variations in a plane through  $\hat{\epsilon}_o$ , and the instrument is rotated about  $\hat{\epsilon}_o$  and the process repeated to measure flux distributions in a sequence of planes. If the temporal stability of flux output by the source is in question, a second detector may be mounted to monitor the source output from a fixed off-axis direction relative to  $\hat{\epsilon}_o$ , *i.e.* by mounting it on an extension to the rotational stage.

Whether one must go to the trouble to determine the beam and FOV weighting functions more accurately than can be modeled from simple geometric elements of the optical design depends on the shape of the VSF in the region to be measured. The detailed behaviour of the outer edges of the two distribution

functions are not important factors in determining the weighting functions for measurements of the VSF of pure water, or of a particulate VSF at scattering angles near, or greater than,  $90^\circ$  (Figs. 1.2 and 1.3). Therefore, relatively simple approximations to  $h_o[\hat{\mathbf{e}} \in \overset{V}{\Omega}_o]$  and  $h_d[\hat{\mathbf{e}} \in \overset{V}{\Omega}_d]$  should be completely adequate for the commercial backscattering instruments mentioned above. Conversely, the angular breadth and details of the beam and FOV distribution functions both become increasingly more critical when one wishes to measure the VSF at decreasing angles in the forward direction.

#### *Dependence of the Weighting Functions on the Beam Attenuation Coefficient $c$*

The effect of the beam attenuation coefficient on the weighting function  $W(\overset{V}{\mathbf{x}}; c)$  for each volume element is explicitly represented in (5.7) by the transmittance over the combined pathlength from the source to the volume element at  $\overset{V}{\mathbf{x}}$  and from there to the source location. The transmittance term is integrated into each angular weighting function  $W(\psi; c)$  determined using (5.8). Strictly speaking, near-forward scattered light still enters  $\Delta V(\overset{V}{\mathbf{x}})$  and can be scattered to the detector (see also the discussion of transmissometer acceptance angles in Chapter 2), but we will neglect this complication in the present discussion. The ratios of integrated weighting functions  $\frac{\int W(\psi; c) \sin \psi d\psi}{\int W(\psi; c=0) \sin \psi d\psi}$  are compared against increasing beam attenuation coefficient  $c$  for the three ECO-VSF weighting functions illustrated in Fig. 5.2. These functions are clearly log-linear, and should we choose to represent the weighting function exclusively using  $W(\psi; c=0)$ , it would be a simple matter to adjust the results for  $c$  dependence. This dependence may either be applied as a correction to the weighting function, or by a transmittance function of the form  $\bar{\beta}_p(\lambda, \bar{\psi}; c) = \bar{\beta}_p(\lambda, \bar{\psi}) \exp[-c r_{\text{eff}}(\bar{\psi})]$ , where  $\bar{\beta}_p(\lambda, \bar{\psi})$  is the measured VSF using  $W(\psi; c=0)$  (see below) and  $r_{\text{eff}}(\bar{\psi})$  is an effective net pathlength for the particular scattering angle measurement.

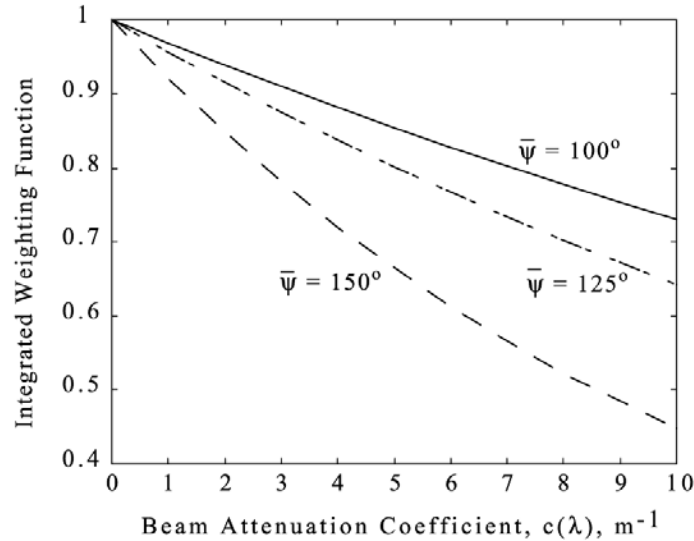


Fig. 5.3: Dependence of the integrated weighting functions  $\int W(\psi; c) \sin \psi d\psi$  on the beam attenuation coefficient for the 3 ECO-VSF weighting functions of Fig. 5.2.

#### *Calibration with Polystyrene Spheres*

In this approach, a sample of polystyrene microsphere beads must be obtained and prepared for use in the calibration procedure. The following procedures are recommended:

1. Assume the bead diameters  $D_p$  in the sample are distributed as a Gaussian probability density function (pdf)  $p(D_p)$  with the mean  $\bar{D}_p$  and standard deviation  $S_D$  provided by the manufacturer; normalize the pdf to unit area.
  - a. It is good practice to occasionally verify the reported mean diameter and standard deviation using a Coulter Counter, or other particle size counting device, for randomly selected samples received from a manufacturer.
2. Calculate the refractive index of the polystyrene spheres relative to pure water

$$n_p(\lambda) = \frac{n_p^{\text{air}}(\lambda)}{n_w(\lambda)}, \quad (5.11)$$

where the particle refractive index relative to air is determined according to a relationship provided by the manufacturer, *e.g.* from Duke Scientific as

$$n_p^{\text{air}}(\lambda) = 1.5663 + 0.00785\lambda^{-2} + 0.000334\lambda^{-4}, \quad \lambda \text{ in } \mu\text{m}, \quad (5.12)$$

and the refractive index of water relative to air is (Austin and Halikas 1976)

$$n_w(\lambda) = 1.325147 + \frac{6.6096}{\lambda - 137.1924}, \quad \lambda \text{ in nm}. \quad (5.13)$$

Note carefully the different wavelength units in the empirical equations (5.12) and (5.13).

3. Calculate the particle scattering phase function for each diameter  $D_p$ , in 500 equally spaced intervals spanning  $\pm 3$  standard deviations about the mean diameter (*i.e.*  $\Delta D_p = \frac{6S_D}{500}$ ), using a Mie (1908) scattering model code (*e.g.* Bohren and Huffman 1983; other coding implementations are also available at various web sites). The Mie scattering intensity functions should be calculated at angle intervals  $\Delta\psi$  matching those at which the weighting functions  $W(\psi; c)$  were resolved [equations (5.8) and (5.9)]. It is important that the selected angle increment adequately resolves variations in  $\beta_{\text{ps}}^0(\lambda, \psi; D_p)$  for the narrow size distributions typically used in this application; an interval  $\Delta\psi \leq 0.5^\circ$  is recommended.
4. Determine the phase function for the sample polydispersion by numerical quadrature of the convolution integral
 
$$\beta_{\text{ps}}^0(\lambda, \psi) = \int \beta_{\text{ps}}^0(\lambda, \psi; D_p) p(D_p) dD_p = \sum_{n=-250}^{250} w_n \beta_{\text{ps}}^0(\lambda, \psi; \bar{D}_p + n\Delta D_p) p(\bar{D}_p + n\Delta D_p) \Delta D_p \quad (5.14)$$
 where  $w_n$  are the weighting coefficients of the selected numerical quadrature algorithm (*e.g.* the composite Simpson formula).
5. To obtain the weighted phase function to be measured by the sensor, divide both sides of (1.19) by  $b(\lambda)$  and numerically approximate the integral equation as

$$\bar{\beta}_{\text{ps}}^0(\lambda, \bar{\psi}) = \sum_{n=-\frac{N_{\Delta\psi}}{2}}^{\frac{N_{\Delta\psi}}{2}} w_n \beta_{\text{ps}}^0(\lambda, \bar{\psi} + n\Delta\psi) W(\bar{\psi} + n\Delta\psi; c) \sin \psi \Delta\psi, \quad (5.15)$$

where again  $w_n$  are the quadrature weighting coefficients.

6. Measure and record the instrument's dark offset response  $V_{\text{dark}}(\bar{\psi})$  by pointing the source and detector at a black velvet cloth, at a distance of approximately 2 m in a completely dark room.
7. Prepare a volume of filtered optically pure water, using the procedures described in Chapter 3.
8. Using an ac-9, calibrate it using the freshly prepared pure water (Chapters 2 and 3).

9. Immerse the VSF sensor in the pure water volume and record its response  $V_w(\bar{\psi}) - V_{\text{dark}}(\bar{\psi})$ .
10. Add a sufficient amount of the polystyrene microsphere bead sample to increase the instrument's response to approximately the maximum level desired for the calibration run.
  - a. Label this bead concentration as C0 and record the VSF sensor response  $V_{C_0}(\bar{\psi})$ .
  - b. Measure  $a_{C_0}(\lambda)$  and  $c_{C_0}(\lambda)$ , relative to the pure water calibration offsets, using the ac-9 for bead concentration C0. Determine  $b_{\text{ps}}^{C_0}(\lambda) = c_{C_0}(\lambda) - a_{C_0}(\lambda)$ , including scattering and temperature corrections to the ac-9 measurements (Chapter 3).
11. Add pure water to dilute the sequence to bead concentration C1 and record the VSF response signal  $V_{C_1}(\bar{\psi})$ , and repeat this step several times to obtain N+1 VSF response signal  $V_{C_0}(\bar{\psi}), V_{C_1}(\bar{\psi}), \dots, V_{C_N}(\bar{\psi})$  corresponding to N+1 bead concentrations. It is not necessary to determine either the absolute, or relative bead concentrations, so dilution volumes of pure water need not be measured. At each dilution concentration Cn, repeat steps 10a and 10b.

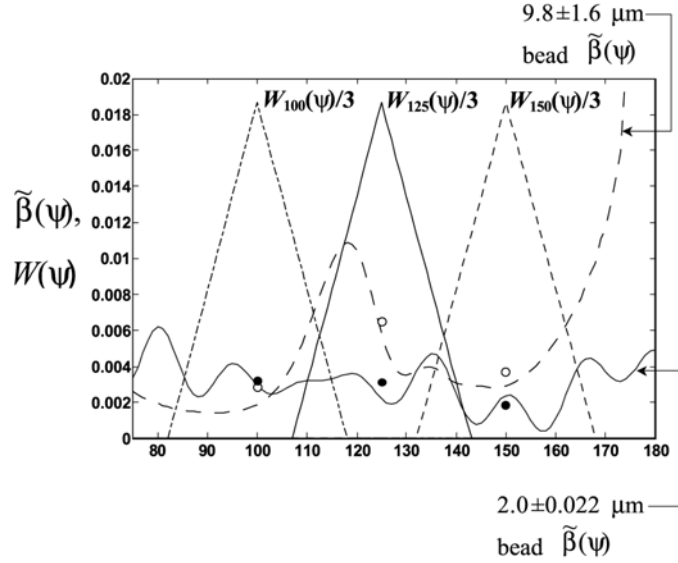


Figure 5.4: Examples of phase functions  $\beta_{\text{ps}}^0(\lambda, \psi)$  calculated using Mie theory for polydispersions of polystyrene microsphere beads having mean diameters of 2  $\mu\text{m}$  (solid line) and 9.8  $\mu\text{m}$  (dashed line), and in both cases relatively small standard deviations. The open and closed circles show the corresponding weighted phase functions  $\bar{\beta}_{\text{ps}}^0(\lambda, \bar{\psi})$  calculated by convolving each phase function with the ECO-VSF weighting functions  $W(\psi)$  illustrated in Fig. 5.2.

The response calibration factor for a given bead concentration C0 to CN is determined as

$$F_{C_n}(\bar{\psi}) = \frac{b_{\text{ps}}^{C_n}(\lambda) \bar{\beta}_{\text{ps}}^0(\lambda, \bar{\psi})}{V_{C_n}(\bar{\psi}) - V_w(\bar{\psi}) - V_{\text{dark}}(\bar{\psi})} \quad (5.16)$$

where the polystyrene sphere phase function  $\bar{\beta}_{\text{ps}}^0(\lambda, \bar{\psi})$  is determined from (5.15). If necessary, the coefficient for each Cn is adjusted for dependence on the beam attenuation coefficient, and the sample is

averaged to obtain the linear calibration coefficient  $F(\bar{\psi})$ . Given VSF measurements  $V_m(\bar{\psi})$  in an unknown natural water mass, the weighted VSF for particles is calculated as

$$\bar{\beta}_p(\lambda, \bar{\psi}) = F(\bar{\psi})[V_m(\bar{\psi}) - V_w(\bar{\psi}) - V_{\text{dark}}(\bar{\psi})]. \quad (5.17)$$

### 5.3 CHARACTERIZATION and CALIBRATION OF A VSF SENSOR USING A REFLECTING PLAQUE

Maffione and Dana (1997) approach the calibration of a VSF sensor by inserting a horizontal plaque of assumed Lambertian reflectance  $\frac{\rho}{\pi}$  into the position of the xy-plane illustrated in Fig. 5.1. Substituting

this reflectance for the VSF in (5.6) and integrating over x and y yields the equation

$$\frac{\Phi_{\text{dp}}[\Delta z; c]}{\Phi_o} = \frac{\rho}{\pi} \iint_{x,y} |\hat{\mathbf{e}}(\hat{\mathbf{x}}_d - \hat{\mathbf{x}}) \cdot \hat{\mathbf{g}}| W(\hat{\mathbf{x}}; c) dx dy = \frac{\rho}{\pi} W_p(z; c), \quad (5.18)$$

representing the total flux reflected from the plaque into the FOV of the detector. If the plaque is moved continuously over z the integral of (5.18) yields the total relative flux reflected from the plaque to the detector from the volume intersection of the source beam and detector FOV as

$$\frac{\Phi_{\text{dp}}[c]}{\Phi_o} = \frac{\rho}{\pi} \int_z W_p(z; c) dz. \quad (5.19)$$

A similar integration of (5.1) yields

$$\frac{\Phi_{\text{dp}}[c]}{\Phi_o} = \iiint_{z,x,y} \beta(\psi(\hat{\mathbf{x}})) W(\hat{\mathbf{x}}; c) dx dy dz = \beta(\psi^*) \int_z W(z; c) dz \quad (5.20)$$

where the angle  $\psi^*$  is selected so that the equality holds; the mean value theorem assures that this must be true for at least one scattering angle. Taking the ratio of (5.19) and (5.20) and solving for  $\beta(\psi^*)$  yields the result

$$\beta(\psi^*) = \frac{\rho}{\pi} \frac{\Phi_{\text{dp}}[c] \int_z W_p(z; c) dz}{\Phi_o \int_z W(z; c) dz}. \quad (5.21)$$

We refer the reader to Maffione and Dana (1997) for the derivation of the unknown terms in (5.21) from the plaque integral and differential measurements, and defer further comparative analysis and description of this method and the explicit approach of Section 5.2 for a future revision to this chapter.

### 5.4 METHODS FOR THE DETERMINATION OF THE BACKSCATTERING COEFFICIENT FROM VSF MEASUREMENTS AT ONE OR MORE SCATTERING ANGLES

If the complete VSF is measured at fine angular resolution using a general angle scattering meter, then it is straightforward to integrate it over the backward hemisphere to determine  $b_b(\lambda)$  directly.

*Determination of  $b_b(\lambda)$  from VSF Measurements at Three or More Angles*

The approach used to determine  $b_b(\lambda)$  from measurements of  $\bar{\beta}(\lambda, \psi_i, \phi)$ ; at  $i=1, 2, K, N$  angles, e.g. using a WET Labs VSF-3, is to fit a polynomial to the  $N+1$  values  $2\pi\bar{\beta}(\lambda, \psi_i, \phi)\sin\psi_i$  derived from

the N measurements and the endpoint  $2\pi\beta(\lambda, \pi, \bullet)\sin\pi \equiv 0$  and integrate it from  $\frac{\pi}{2}$  to  $\pi$  (following Beardsley and Zaneveld 1969).

#### *Determination of $b_b(\lambda)$ from VSF Measurements at Only One Angle*

Oishi (1990) used Mie scattering calculations and VSF observations to determine  $\beta^n(\lambda, \psi)$  and  $b_b^n(\lambda)$  for polydispersions of spheres having different size distributions similar to those observed for marine hydrosols. He invoked the mean value theorem to observe, from the definition of  $b_b(\lambda)$ , that for each  $n^{\text{th}}$  polydispersion phase function  $\beta^b(\lambda, \psi)$  there must be at least one angle  $\psi_n^*$  for which

$$b_b^n(\lambda) = 2\pi\beta^n(\lambda, \Psi_n^*) \int_{\frac{\pi}{2}}^{\pi} \sin\Psi d\Psi = 2\pi\beta^n(\lambda, \Psi_n^*) .^2 \quad (5.22)$$

Oishi (1990) then further observed that for a selected common reference angle  $\psi^*$ , he could determine an approximate linear estimate of the backscattering coefficient for each polydispersion as

$$\hat{b}_b^n(\lambda) \approx 2\pi\chi(\Psi^*)\beta^n(\lambda, \Psi^*), \quad (5.23)$$

where the coefficient  $\chi(\Psi^*)$  is selected to minimize the uncertainty

$$U(\Psi^*) = \sqrt{\frac{\sum_{n=1}^N [b_b^n(\lambda) - \hat{b}_b^n(\lambda)]^2}{N}} . \quad (5.24)$$

By varying  $\psi^*$ , Oishi found that the minimum overall uncertainty for the ensemble of N size distributions occurred at  $\psi^* = 120^\circ$ , with  $\chi(120^\circ) = 1.14$ .

Boss and Pegau (2001) separated the VSF and backscattering coefficient as

$$\begin{aligned} \beta(\lambda, \Psi) &= \beta_w(\lambda, \Psi) + \beta_p(\lambda, \Psi) \text{ and} \\ b(\lambda) &= b_w(\lambda) + b_b(\lambda), \end{aligned} \quad (5.25)$$

where the subscripts ‘‘p’’ and ‘‘w’’ designate contributions due to particles and water, respectively. The scaling factor  $\chi(\Psi^*)$  is correspondingly partitioned as

$$\chi(\Psi^*) = \chi_p(\Psi^*) \frac{\beta_p(\lambda, \Psi^*)}{\beta(\lambda, \Psi^*)} + \chi_w(\Psi^*) \frac{\beta_w(\lambda, \Psi^*)}{\beta(\lambda, \Psi^*)}. \quad (5.26)$$

Analyses similar to those of Oishi (1990) and Maffione and Dana (1997), but in this partitioned framework, led Boss and Pegau (2001) to conclude that  $\chi(\Psi^*) = \chi_p(\Psi^*) = \chi_w(\Psi^*) \cong 1.1$  only when  $\Psi^* = 117^\circ \pm 3^\circ$ , consistent with the results of Oishi (1990). For measurements at other scattering angles, they recommend modifying Equation (4.6) to correct for the water scattering contribution as

$$\hat{b}_b(\lambda) = 2\pi\chi_p(\Psi^*)[\beta(\lambda, \Psi^*) - \beta_w(\lambda, \Psi^*)] + b_{bw}(\lambda). \quad (5.27)$$

They provide equations for estimating  $\beta_w(\lambda, \Psi)$  and  $b_w(\lambda)$ , based on the theoretical equations and experimental results of Morel (1974), and tabulate estimates of  $\chi_p(\Psi^*)$  in the range  $90^\circ \leq \Psi^* \leq 170^\circ$ .

## REFERENCES

---

<sup>2</sup> Recalling that  $\beta(\lambda, \psi) = b(\lambda)\beta^b(\lambda, \psi)$  [Vol. I, Ch. 2, Sect. 2.4].

- Beardsley, G.F. and J.R.V. Zaneveld, 1969: Theoretical dependence of the near-asymptotic apparent optical properties of sea water. *J. Opt. Soc. Amer.* **59**: 373-377.
- Bohren, C.F., and D.R. Huffman, 1983: *Absorption and Scattering of Light by Small Particles*, Wiley, New York, 530pp
- Boss, E. and W.S. Pegau, 2001: Relationship of light scattering at an angle in the backward direction to the backscattering coefficient. *Appl. Opt.*, **40**: 5503-5507.
- Mie, G., 1908: Beitrage zur Optic truber Medien, speziell kolloidalen Metallosungen, *Ann. Phys.*, **25**: 377-442.
- Maffione, R.A. and D.R. Dana, 1997: Instruments and methods for measuring the backward-scattering coefficient of ocean waters. *Appl. Opt.* **36**: 6057-6067.
- Mobley, C.D., L.K. Sundman, and E. Boss, 2002. Phase function effects on oceanic light fields. *Appl. Opt.*, **41**(6): 1035-1050.
- Oishi, T., 1990. Significant relation between the backward scattering coefficient of sea water and the scatterance at 120 degrees. *Appl. Opt.*, **29**(31): 4658-4665.
- Petzold, T.J., 1972. Volume scattering functions for selected ocean waters. Contract No. N62269-71-C-0676, UCSD, SIO Ref. 72-78.
- Stramska, M., D. Stramski, B.G. Mitchell and C.D. Mobley. 2000: Estimation of the absorption and backscattering coefficients from in-water radiometric measurements. *Limnol. Oceanogr.*, **45**: 628-641.
- Zaneveld, J.R.V., 1982: Remotely sensed reflectance and its dependence on vertical structure: a theoretical derivation. *Appl. Opt.*, **21**(22): 4146-4150.